Vortices in ferromagnetic elements with perpendicular anisotropy

C. Moutafis, S. Komineas, C. A. F. Vaz, and J. A. C. Bland
Cavendish Laboratory, J J Thomson Avenue, Cambridge CB3 0HE, United Kingdom

P. Eames
NVE Corporation, 11409 Valley View Road, Eden Prairie, Minnesota 55344, USA

(Received 21 April 2006; revised manuscript received 31 July 2006; published 7 December 2006)

We study equilibrium properties of disc-shaped ferromagnetic elements with perpendicular anisotropy and quality factor less than unity. A vortex is a static state for sufficiently thin particles. For thicker particles we find a continuous transition to a bidomain state which is stable for a range of particle diameters. This bidomain state is akin to a magnetic "bubble" where the magnetization is directed along the symmetry axis at the center of the disc and it is oppositely magnetized at the periphery. The magnetization profile of the bidomain state presents the same winding around the symmetry axis as the vortex. Its signature is its magnetostatic field which consists of two concentric regions of opposite sign above the particle top surface. Higher-order states of multiple concentric domains with alternating magnetization direction are also found for particles of sufficiently large lateral dimensions. Finally, we explain how these ideas apply to particles with a very small perpendicular anisotropy.

DOI: 10.1103/PhysRevB.74.214406 PACS number(s): 75.75.+a, 75.60.Ch, 75.70.Kw

I. INTRODUCTION

Magnetic materials with a uniaxial magnetocrystalline anisotropy perpendicular to the surface of the magnetic element are becoming increasingly important in many areas of applied and theoretical research. Recently, mesoscopic elements with perpendicular anisotropy have been found to display a rich variety of magnetization patterns. In a series of experiments with cylindrical cobalt dots magnetic domains were often observed to form remarkably regular patterns.[1] The magnetic domain structure of nickel dots was found to present similar patterns,[2] which were also revealed in micromagnetic studies.[3] It thus appears that the situation for high-symmetry magnetic domain states is significantly richer in perpendicular anisotropy particles compared to isotropic ones. Therefore these constitute an excellent system for theoretical studies. The interest in the subject is also due to the potential for applications, mainly in the context of magnetic recording technology. High-density magnetic recording will be based on perpendicular anisotropy materials, which allow for a substantial increase of storage densities.

Most of the past research effort on mesoscopic magnetic elements has focused on materials with negligible or with a small in-plane anisotropy where the vortex appears to be dominant.[4] Permalloy is an example of a widely used material in this research area. The situation appears to change dramatically for permalloy dots with a very weak deposition induced perpendicular anisotropy which were studied in Ref. 5. Instead of a single vortex, a variety of domain patterns were observed which have an MFM (magnetic force microscopy) signature similar to the one in higher anisotropy dots.[1,2] This indicates that the perpendicular component of the magnetization is significantly more complicated than the simple vortex state observed in dots of similar size but with a vanishing anisotropy.

Circular magnetic domains of high symmetry were observed in many of the above-mentioned experiments and these appear to be akin to magnetic bubbles which have been thoroughly studied in high perpendicular anisotropy continuous films.[6] The relevance of a magnetic bubble for mesoscopic magnetic elements has been pointed out in Ref. 7 where it was argued that this can form the ground state of disc-shaped particles with high perpendicular anisotropy. A systematic study of the domain patterns and the magnetic states in perpendicular anisotropy elements, such as the ones used in the experiments mentioned above, has not been given yet. In this paper we study disc-shaped particles with a quality factor less than unity. A vortex can be found in sufficiently thin particles. Thicker particles can sustain highly symmetric bidomain and multidomain states. We discuss the relation of bidomain states to magnetic bubbles while axially symmetric tridomain states are viewed as their generalizations.

The paper is organized as follows. In Sec. II we describe in detail a vortex in a very thin disc-shaped particle. In Sec. III we study axially symmetric bidomain and tridomain states in particles with a quality factor as in hcp Co and in the tetragonally distorted Ni(001). In Sec. IV we show the relevance of our ideas for the permalloy dots studied in Ref. 5. Finally, Sec. V contains our conclusions.

II. VORTICES IN THIN DOTS

We consider a disc-shaped particle of thickness t and radius R. We suppose a uniaxial magnetocrystalline anisotropy with the easy axis along the symmetry axis of the particle which is taken to be the z axis. Statics and dynamics of the magnetization $\boldsymbol{M}$ are described by the Landau-Lifshitz equation. A natural length scale in the equation is the exchange length $\ell_{\mathrm{ex}}=\sqrt{A/2\pi M_0^2}$, where A is the exchange interaction constant and M_0 is the saturation magnetization. Another important quantity is the dimensionless quality factor $Q=K/2\pi M_0^2$, where K is the uniaxial anisotropy constant. The quality factor is a measure of the relative strength of the magnetostatic and anisotropy interactions. It also enters in

the calculations of the domain-wall width, $\ell_{ex}/\sqrt{Q}$. In the following we shall use ℓ_{ex} as the unit of length and all fields will be scaled to $4\pi M_0$ (and energy per volume to $4\pi M_0^2$). We define

$$\boldsymbol{m} \equiv \frac{\boldsymbol{M}}{M_0}, \quad \boldsymbol{h} \equiv \frac{\boldsymbol{H}}{4\pi M_0}, \tag{1}$$

as the normalized magnetization and magnetostatic field, respectively. We use cylindrical coordinates, where the magnetization components are $\boldsymbol{m}=(m_\rho, m_\phi, m_z)$ and correspondingly $\boldsymbol{h}=(h_\rho, h_\phi, h_z)$. Important in the following is the anisotropy energy which is typically considered to be modelled by an on-site term and, following our scaling conventions, it has the form

$$E_a = \frac{Q}{2}\int (1-m_z^2)dV, \tag{2}$$

where the integration extends over the particle volume.

Our aim is to find the equilibrium magnetic states in the particle, which are the static solutions of the Landau-Lifshitz equation. As a starting point we take the limit of a very thin particle. This has been rigorously defined in Ref. 8, where it is proved that the magnetization does not vary along the thickness. One needs to minimize a two-dimensional Hamiltonian, which is achieved by substituting an effective perpendicular anisotropy term $E_m^{(\mathrm{eff})}=t/2\int m_z^2 dxdy$ for the nonlocal magnetostatic energy term. Therefore, in the very thin limit, the energy includes the following total effective anisotropy term:

$$E_a + E_m^{(\mathrm{eff})} = \frac{1-Q}{2} t \int m_z^2 dxdy + \mathrm{const.} \tag{3}$$

We consider throughout this paper that Q is positive and less than unity, $Q<1$. Thus Eq. (3) implies that z is a hard axis, and the lowest energy state is a uniform magnetization state with $\boldsymbol{m}$ lying on the (x,y) plane.

Numerous experiments have reported a vortex in disc particles. Observations of vortices were reported in Refs. 9 and 10, and vortices and antivortices in rectangular particles were reported in Ref. 11. Vortex states in cubic particles have been studied in Ref. 12, and a theoretical study of the stability of a vortex in a disc particle was given in Ref. 13. Studies on vortices or swirls in particles are reviewed in Ref. 14.

We assume here that a vortex is a static solution even in the very thin limit. The radius of the vortex core is inversely proportional to the root of the effective anisotropy constant $R_{\mathrm{core}} \sim \ell_{ex}/\sqrt{1-Q}$. One can obtain a more precise result by employing Eq. (A3) given in the Appendix. If we use the simple model for the vortex (ρ_0 a parameter),

$$m_\rho = 0, \quad m_\phi = \tanh(\rho/\rho_0), \quad m_z = 1/\cosh(\rho/\rho_0), \tag{4}$$

and substitute in Eq. (A3), we find

$$\rho_0 = 0.85/\sqrt{1-Q}. \tag{5}$$

In order to verify the above results but also to calculate the vortex away from the very thin limit we solve the Landau-Lifshitz equation by our numerical code which explicitly imposes axial symmetry, thus being ideal for calculating static axially symmetric states in a disc particle. We thus suppose

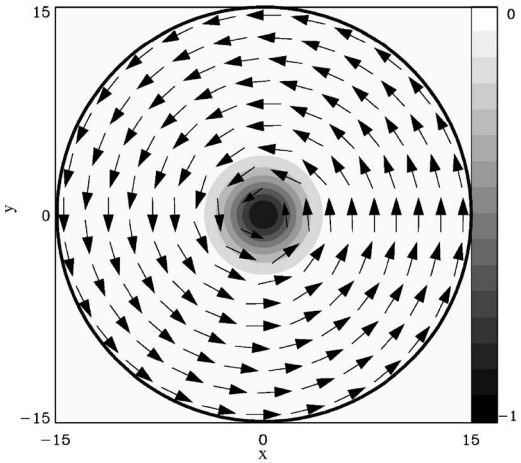

FIG. 1. The vortex profile at the top of a disc particle with radius $R=15.1$, thickness $t=3.1$, and quality factor $Q=0.4$. The arrows show the projection of the magnetization vector $\boldsymbol{m}$ on the (x,y) plane while the third component of the magnetization (m_z) is coded in gray scale. The magnetization at the center is $m_z=-1$. There is little variation of the magnetization across the thickness. In this and following figures length is measured in exchange length units.

$$m_\rho = m_\rho(\rho,z), \quad m_\phi = m_\phi(\rho,z), \quad m_z = m_z(\rho,z), \tag{6}$$

which implies

$$h_\rho = h_\rho(\rho,z), \quad h_\phi = 0, \quad h_z = h_z(\rho,z). \tag{7}$$

In our numerical simulations we have chosen $Q=0.4$ which corresponds to both hcp Co and to tetragonally distorted Ni(001). We note, however, that these materials have different exchange lengths $\ell_{ex}=2.85$ and 8.3 nm, respectively. Our algorithm converges to a static axially symmetric vortex when the particle is thin ($t \leqslant 5\ell_{ex}$) and has a radius much larger than the vortex core. The results are consistent with Eq. (5) although satisfying this to a good accuracy would require an extremely thin particle ($t<\ell_{ex}$). We present in Fig. 1 the numerical result for a vortex in a particle with thickness $t=3.1$ and radius $R=15.1$. The magnetization at the top surface of the disc is shown and there is only little variation of $\boldsymbol{m}$ across the particle thickness, as is expected in the very thin limit. Approximating the profile in Fig. 1 by the model (4) we find $\rho_0=1.9$, which is much larger than the value (5) obtained in the very thin limit. We thus stress that the vortex core radius increases significantly with the particle thickness. The virial relation (A2) is satisfied by all numerically calculated vortex solutions presented here. This serves also as a check for the accuracy of our numerical results.

The profile of the vortex in Fig. 1, as well as all magnetic configurations presented in this paper, satisfy the parity relations

$$m_\rho(\rho,z) = -m_\rho(\rho,-z), \quad m_\phi(\rho,z) = m_\phi(\rho,-z),$$

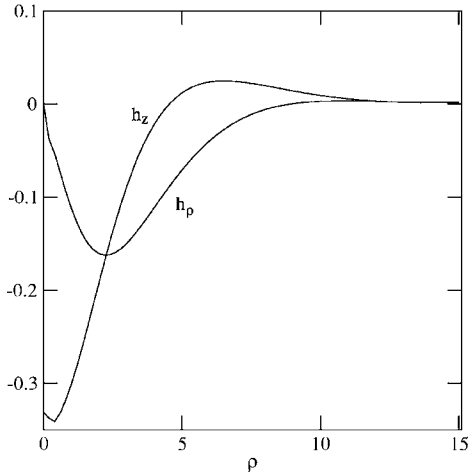

FIG. 2. The magnetostatic field $\boldsymbol{h}$ of the vortex in Fig. 1 just over the top particle surface. The field is axially symmetric and we present the two nonzero components h_ρ, h_z as functions of the radial coordinate ρ.

$$m_z(\rho,z) = m_z(\rho,-z). \tag{8}$$

Of significant practical importance is the magnetostatic field produced by the vortex. We plot in Fig. 2 its two nonvanishing components h_ρ, h_z above the top particle surface. The component h_z has an extremum at the vortex center, while h_ρ has a significant value at the tail of the vortex core, while it vanishes at the center. The magnetostatic field vanishes away from the vortex core, as expected.

We conclude this section by considering the vortex for varying particle radius. For large radii it is clear that the vortex remains a solution and its core remains unchanged. On the other hand, as the radius of the particle becomes very small and comparable to the vortex core size the vortex is reduced to its core and it actually becomes similar to a single domain (SD) along the symmetry axis. This situation is further discussed in Sec. IV.

III. BIDOMAIN STATES

We now consider particles of increasing thickness and investigate how the picture described in the previous section is modified. Figure 3 shows the result of a numerical calculation for radius $R=15.1$ and thickness $t=11$. We have two concentric domains: the central domain points down and the outer domain points up (the state obtained by $\boldsymbol{m}\rightarrow-\boldsymbol{m}$ is a solution, too). The domain wall between the two domains is Bloch-like at the central plane (upper panel). The magnetostatic (stray) field causes the magnetization to develop a large m_ρ component at the domain wall near the top and bottom surfaces where this becomes Néel-like and its width is on the order of the particle radius (lower panel). Figure 3 shows that this bidomain state retains many of the features of a vortex. In particular, the magnetization vector winds around a full circle about the symmetry axis z. A cross section of the dot is shown in Fig. 4. Since this is an axially symmetric configuration the three-dimensional picture is generated by a revolution of the figure around the z axis.

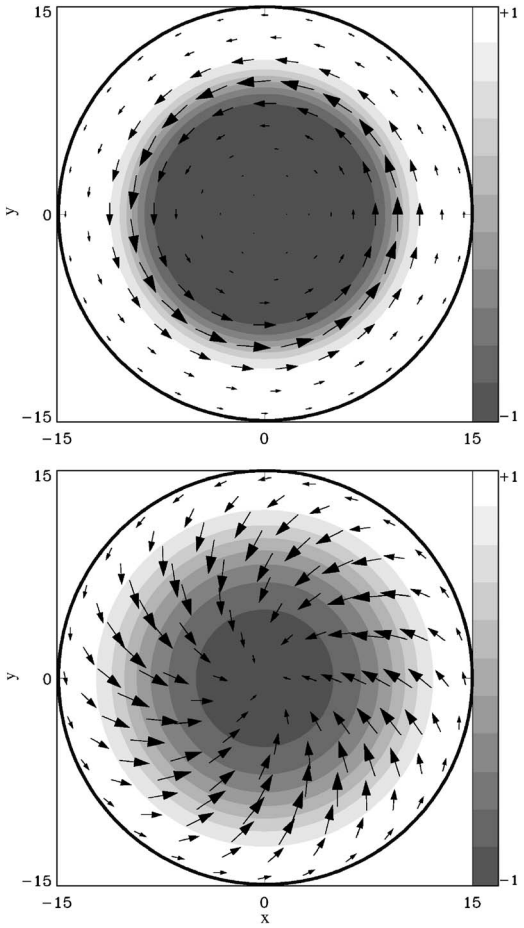

FIG. 3. The bidomain state ("monobubble") illustrated in the middle plane (upper panel) and at the top (lower panel) of a disc particle with radius $R=15.1$, thickness $t=11$, and quality factor $Q=0.4$. The picture at the bottom surface is inferred by Eq. (8). The magnetization is $m_z=-1$ at the center and $m_z\approx 1$ in the outer domain. The arrows show the projection of the magnetization on the (x,y) plane, while the third component (m_z) is coded in gray scale. Note that the gray scale code adopted here is different from that in Fig. 1.

This bidomain state has been observed in Ni dots.[2] For the case of hcp Co, states of weak circular stripe domain as the one in Fig. 3 have been studied numerically in Ref. 15. Finally, we note that the virial relation (A2) is satisfied for our solution, and for all subsequent calculations presented in this section, to an accuracy better than 2%.

We shall call the magnetic state in Fig. 3 a "monobubble" since it can be viewed as a single magnetic bubble in a particle. Magnetic bubbles have been discussed extensively in the context of films with perpendicular anisotropy where they exist only in the presence of an external magnetic bias field.[6] On the other hand, it has been shown in Ref. 7 that magnetic bubbles exist in particles with high perpendicular anisotropy $(Q>1)$ also in the absence of any external bias field. In the present case $(Q<1)$ the bidomain state profile differs from the above-mentioned cases in that it is here dominated by the domain wall which extends over an area on the order of the particle size.

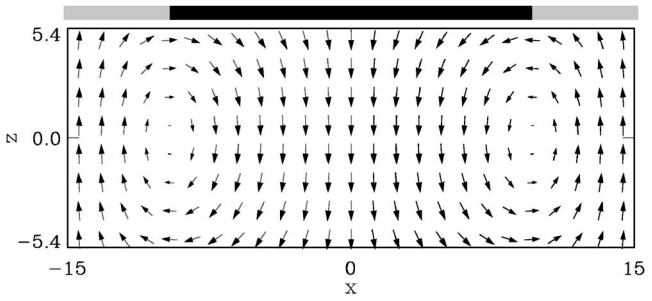

FIG. 4. A cross section across the particle diameter for the monobubble shown in Fig. 3. The arrows show the projection of the magnetization on the cross section (m_ρ and m_z shown). The bar on the top color codes the sign of h_z just over the top dot surface. Black indicates negative and gray indicates positive values.

The magnetostatic field of the monobubble of Figs. 3 and 4 is presented in Fig. 5. We plot the two nonvanishing components h_ρ, h_z above the top particle surface. The third component h_z has opposite signs between the central and the outer domain reflecting the perpendicular component of the magnetization. The sign of h_z is also shown in Fig. 4 coded in black and gray color in the bar over the particle. The radial component h_ρ has a significant value at the monobubble domain wall and near the particle side surface.

In order to explore the transition from a vortex to a monobubble we have numerically calculated the magnetic states for a particle radius $R=15.1$ and thickness range $2<t<11$. We find a vortex for $t<5$ and a monobubble for $t>7$. For $5<t<7$ the state is intermediate between the two. The smooth transition between the two states is made obvious in Fig. 6 where we plot the total magnetization per unit volume along the symmetry axis ($V=\pi R^2 t$ is the particle volume)

$$\mu \equiv \frac{1}{V}\int m_z dV, \tag{9}$$

for varying thickness t of the particle. For $t<5$ only the vortex core magnetization has an out-of-plane component

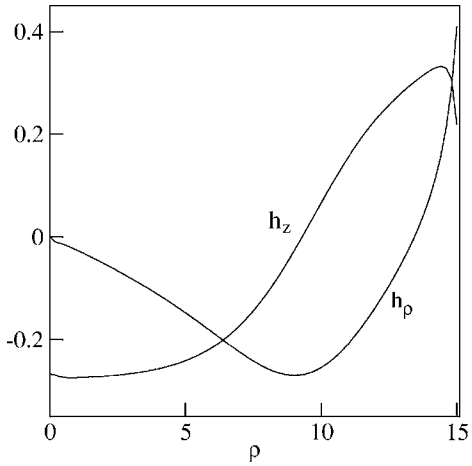

FIG. 5. The magnetostatic field $\boldsymbol{h}$ of the monobubble in Figs. 3 and 4 just above the top particle surface. The field is axially symmetric and we present the two nonzero components h_ρ, h_z as functions of the radial coordinate ρ.

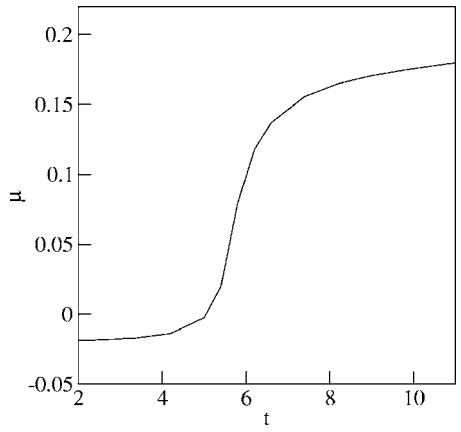

FIG. 6. The total magnetization μ [in units of M_s, defined in Eq. (9)] of a particle with radius $R=15.1$ and varying thickness t (in units ℓ_{ex}). We have a vortex for $t<5$, a monobubble for $t>7$, and an intermediate state for $5<t<7$.

and contributes to μ which has a small value. According to our conventions $m_z<0$ at the vortex core and thus $\mu<0$. In the case of the monobubble the magnetization is out of plane across the particle. The central region is smaller than the outer region due to the domain-wall tension.[7] As a result the total magnetization has a significant net magnetization $\mu>0$. In Ref. 16 a theory was developed for the critical thickness for the tilting of the spins out of plane in a continuous film with perpendicular anisotropy. For $Q=0.4$ the critical thickness was calculated to be $6\ell_{ex}$. This number is indeed in the region where the vortex is turning to a monobubble according to Fig. 6.

We complete the discussion of this section by considering the effect of varying the particle lateral dimension. In Fig. 7

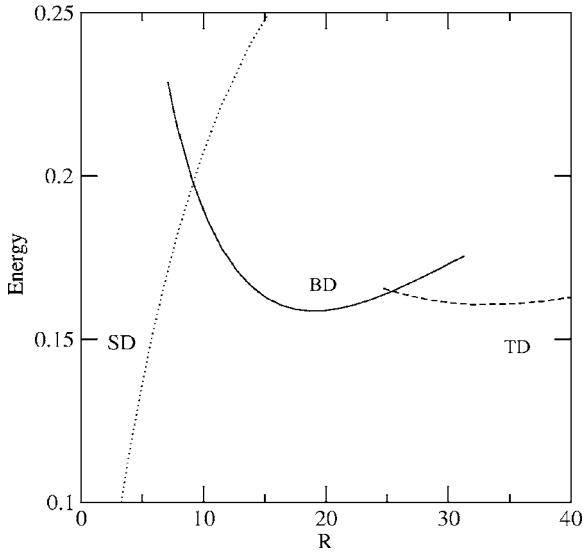

FIG. 7. Energy per unit volume (in units of $4\pi M_0^2$) of the single-domain (SD, dotted line), the monobubble [bidomain (BD), solid line], and the three-ring state [tridomain (TD), dashed line] as a function of disc radius R. The disc thickness is $t=11$, and the quality factor $Q=0.4$. The critical radii R_{c1}, R_{c2} (see text) correspond to the intersections of the dotted and solid lines, and solid and dashed lines, respectively.

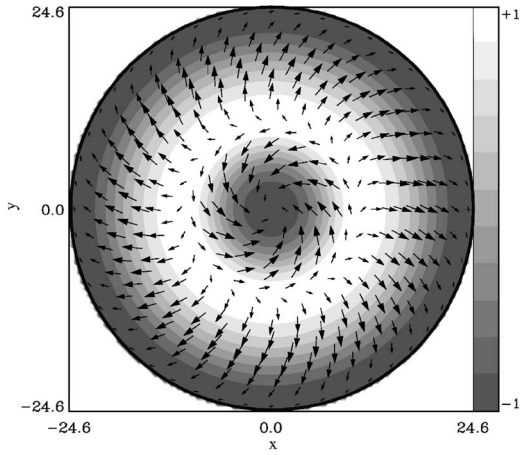

FIG. 8. A tridomain (three-ring) state illustrated at the top surface of a dot with thickness $t=11$, radius $R=24.6$, and a quality factor $Q=0.4$. Arrows show the projection of the magnetization on the plane and m_z is coded in gray scale.

we present the energies of the various axially symmetric magnetic states supported in the particle of thickness $t=11$ as a function of radius R. A single-domain (almost uniform) state, pointing along z, is the lowest energy state for small R (dotted line in figure), but its energy increases rapidly with R. The monobubble state (solid line in figure) exists for radii in the range $7<R<31$, while it has energy lower than the single domain for $R>R_{c1}=9$. A similar behavior has been discussed in Ref. 7 for high anisotropy particles; however, the present monobubble state does not exist for very large radii: as indicated in Fig. 7, the solid line terminates at $R=31$.

For particles of sufficiently large lateral dimensions we find higher-order multidomain states. An axially symmetric tridomain state is shown in Fig. 8 and it will be called a "three-ring" state. The sequence of three-ring states for $t=11$ is denoted by a dashed line in Fig. 7. They exist for $R>R_2=22$, they become the lowest energy states for $R>R_{c2}=25.5$, and they should cease to exist for a larger radius (not presented here). Multidomain states in Co dots have been observed in Ref. 1 and the sequence of concentric multidomain states has been further studied and discussed in Refs. 3 and 17.

IV. VERY WEAK ANISOTROPY

Experiments with $Ni_{81}Fe_{19}$ disc particles have been reported in Ref. 5 where bidomain and tridomain states resembling those described in the previous section were observed. The permalloy is known to have a very weak deposition induced perpendicular anisotropy.[18] The diameters of the dots ranged in half integer and integer multiples of the stripe domain size in unpatterned films and the thickness was 190 nm. The magnetic structures were observed with MFM and were found to be dependent on the field history of the samples. Particles with diameters 750 and 850 nm, roughly twice the stripe period width observed in unpatterned samples, show remanent states of two and three concentric

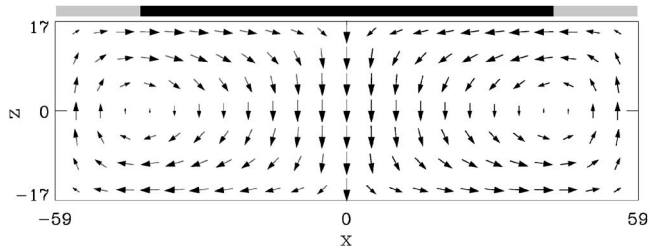

FIG. 9. The bidomain state profile in a cross section across the dot diameter for a particle with radius $R=59.25$, thickness $t=33.5$, and quality factor $Q=0.05$. The arrows show the projection of the magnetization on the cross section (m_ρ and m_z shown). The bar on the top color codes the sign of h_z just over the top dot surface. Black indicates negative and gray indicates positive values.

domains of alternating contrast, respectively. This indicates that the perpendicular component of the magnetization is significantly more complicated than the simple vortex state observed in dots of similar size without the perpendicular anisotropy.

In order to investigate the effect of a low anisotropy we have repeated the procedure of the previous section using now small quality factors. Given an exchange length $\ell_{ex}\approx 5.7$ nm for the permalloy we have chosen a thickness $t=33.5\ell_{ex}$ for the particles in order to match the experiment.[5] We have tried several values for the quality factor and have concluded that $Q=0.05(\pm 0.01)$ give the best agreement with the experimental results. For this Q the results of Ref. 16 suggest a critical thickness for the magnetization tilting out of plane of $23\ell_{ex}$. We note that previous studies on permalloy films with the composition $Fe_{82}Ni_{18}$ have reported the critical thickness for stripe domain nucleation to be 280 ± 30 nm,[19] and this implies a quality factor $Q=0.012$ according to numerical results.[20]

We have performed numerical calculations for radii $R<85(\approx 1\ \mu\text{m})$. We present in Fig. 9 a cross section of a particle with radius $R=59.25$ (diameter 680 nm) in a bidomain (monobubble) state. This is in many respects similar to the one shown in the previous section in Fig. 4, although in the present case the magnetization vector is tilted only slightly out of plane near the particle top and bottom surfaces. Despite the small tilting of the magnetization the magnetostatic field over the particle surface varies significantly. The perpendicular component (h_z), which is important for MFM measurements, changes sign across the particle diameter as shown in black-gray code in Fig. 9. The magnetostatic field components over the particle surface are shown in Fig. 10. The value of h_z is small ($h_z\approx\pm 0.02$ in units of $4\pi M_s$) over most of the disc surface but it is large at the particle center.

An overview of our results is given in Fig. 11 which shows the energy per unit volume of all magnetic states found as a function of the particle radius. A single-domain state exists for small radii (dotted line in the figure). The bidomain state (solid line) is stable for $R<66$ (diameter 750 nm) while its energy has a minimum at $R=45$ (diameter 510 nm). A tridomain state (dashed line) is composed of three concentric domains, similar to the one shown in Fig. 8, and it is stable for $R>55$ (diameter 630 nm) (it should cease

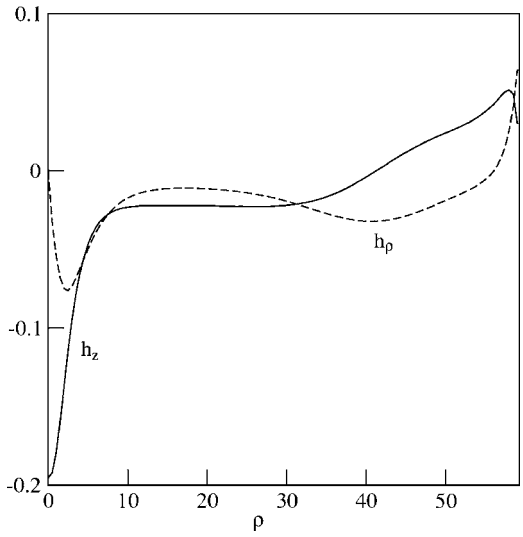

FIG. 10. The magnetostatic field $\boldsymbol{h}$ over the top particle surface for the state shown in Fig. 9 as a function of the distance from the center ρ of the dot.

to exist for some radius larger than 85, not presented here). These results are in agreement with the experimental results in Ref. 5 where the bidomain state was observed in dots with diameters of 600 and 750 nm, while the three-ring state was observed in dots with diameters 850 nm.

We complete this section with a discussion of the details of the solid curve in Fig. 11. The energy density shown by the solid curve increases significantly for small R and this is associated with a qualitative change of the bidomain state. For $R<20$ its outer domain is reduced and the state resembles a vortex with a small flux closure domain. Further reducing the radius ($R<10$) the vortex tail is reduced and eventually the magnetic state is almost uniform along the disc axis, and could thus be described as a single domain.

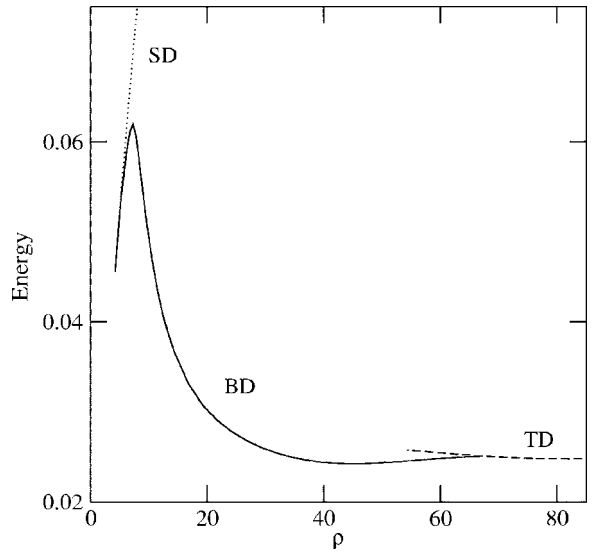

FIG. 11. Energy per unit volume (in units of $4\pi M_0^2$) of the single-domain (SD, dotted line), the bidomain (BD, solid line), and the three-ring state (TD, dashed line) as a function of disc radius R, for thickness $t=33.5$ and a quality factor $Q=0.05$.

For $R<10$ the solid curve approaches the dotted one (SD) but the two lines do not join. As a result, for small radii the solid and dotted curves represent two similar but distinct single-domain states. In order to test whether these two states can actually be distinguished in magnetic elements, we suggest that they should behave differently under the application of an external field along the symmetry axis: one should remain almost uniform while the other should give a vortex whose core is shrinking as the field intensity increases.

V. CONCLUSIONS

We have presented an extensive study of the domain structure of mesoscopic magnetic dots with perpendicular anisotropy corresponding to quality factor (Q) values typical for hcp Co or tetragonally distorted Ni(001). A vortex is typically found in thin dots while the magnetic structure becomes richer in thicker particles where the magnetization tilts out of plane across the particle. A bidomain state is found which is akin to a magnetic bubble, and multidomain states of concentric rings with alternating magnetization are found in dots with larger lateral dimensions. The picture is similar in dots of permalloy with a very small deposition induced perpendicular anisotropy, but the out-of-plane structures are weak and are observed only in thick dots. We have elaborated on the fact that the magnetization profile of the bidomain bubble state presents the same winding around the symmetry axis as the vortex. This is particularly evident in the permalloy case where a vortex is continuously transforming to a bidomain bubble as the lateral dimensions of the dot increase.

Our study applies to small enough particles as indicated, e.g., in Fig. 7 which shows dot radii $R \leqslant 40\ell_{ex}$. On the other hand, the situation in particles with large lateral dimensions is expected to be similar to continuous films where stripe domains prevail. The latter domain structure can be considered as the large radii limit of the problem. However, we have not attempted to study the details of the transition from one limit to the other.

The magnetization configuration of each of the states discussed in this paper presents a certain complexity (as evidenced, e.g., from Figs. 3 and 8), and we have discussed the analogies of the present structures with the magnetic vortex. In particular, both vortices and bubbles are characterized by a topological number. The latter is linked to the magnetization dynamics which, in turn, has proved surprising and interesting in many experimental and theoretical studies of vortex dynamics and of related spin waves and eigenmodes.[21–26] It would be interesting to study the dynamics of the monobubbles and three-ring states discussed in the present paper. The scope of such studies could eventually prove significantly wide. In addition to the structures discussed in this paper one could also envisage bubble states with various topological numbers including zero. Such complicated bubbles would present a varying number of Bloch lines, i.e., they present domain walls of different types. Vortex states with Bloch lines have been observed in ring-shaped particles in Ref. 27.

ACKNOWLEDGMENTS

C.M. was supported by the Cambridge European Trust, Emmanuel College (Cambridge), and Cambridge Philosophical Society. S.K. was supported by EPSRC Grants No. GR/R96026/01 and No. GR/S61263/01.

APPENDIX: VIRIAL THEOREM

A generalization of the well-known Derrick relation for a ferromagnet was derived in Ref. 28 which is now valid for axially symmetric solutions in disc-shaped ferromagnetic elements of any size. We repeat here the result in the form that is used in the present paper. We denote by

$$W_e = \int w_e dV, \quad w_e = \frac{1}{2}\partial_i \boldsymbol{m} \cdot \partial_i \boldsymbol{m},$$

$$W_a = \int w_a dV, \quad w_a = \frac{Q}{2}(1 - m_z^2),$$

$$W_m = -\frac{1}{2}\int \boldsymbol{h} \cdot \boldsymbol{m} dV, \tag{A1}$$

the exchange, anisotropy, and magnetostatic energies, respectively. Using Eq. (8) the Derrick relation reads

$$W_e + 3(W_a + W_m) = 2\pi R^2 \int_{S_R} \left(w_e + w_a - \boldsymbol{h} \cdot \boldsymbol{m} - \frac{1}{2} m_\rho^2 \right) dz + t \int_{S_\pm} \left(w_e + w_a - \boldsymbol{h} \cdot \boldsymbol{m} - \frac{1}{2} m_z^2 \right) 2\pi\rho d\rho, \tag{A2}$$

where S_R is the side surface of the disc, and $S_\pm$ is either of the top or bottom disc surfaces.

In the very thin limit, we suppose that there is no variation along the z axis; also $h_\rho = 0$, $h_z = -m_z$,[8] and $m_\phi(\rho = R) = \pm 1$, which we substitute in Eq. (A2) to obtain

$$\int m_z^2 2\pi\rho d\rho = \frac{\pi}{1 - Q}. \tag{A3}$$

This equation can also be obtained by employing a result given in the Appendix of Ref. 29.

[1] M. Hehn, K. Ounadjela, J.-P. Bucher, F. Rousseaux, D. Decanini, B. Bartenlian, and C. Chappert, Science **272**, 1782 (1996).
[2] G. D. Skidmore, A. Kunz, C. E. Campbell, and E. D. Dahlberg, Phys. Rev. B **70**, 012410 (2004).
[3] J. Kin Ha, R. Hertel, and J. Kirschner, Europhys. Lett. **64**, 810 (2003).
[4] M. Kläui, C. A. F. Vaz, L. Lopez-Diaz, and J. A. C. Bland, J. Phys.: Condens. Matter **15**, R985 (2003).
[5] P. Eames and E. D. Dahlberg, J. Appl. Phys. **91**, 7986 (2002).
[6] A. P. Malozemoff and J. C. Slonczewski, *Magnetic Domain Walls in Bubble Materials* (Academic, New York, 1979).
[7] S. Komineas, C. A. F. Vaz, J. A. C. Bland, and N. Papanicolaou, Phys. Rev. B **71**, 060405(R) (2005).
[8] G. Gioia and R. James, Proc. R. Soc. London, Ser. A **453**, 213 (1997).
[9] T. Shinjo, T. Okuno, R. Hassdorf, K. Shigeto, and T. Ono, Science **289**, 930 (2000).
[10] J. Raabe, R. Pulwey, R. Sattler, T. Schweinböck, J. Zweck, and D. Weiss, J. Appl. Phys. **88**, 4437 (2000).
[11] K. Shigeto, T. Okuno, K. Mibu, and T. Shinjo, Appl. Phys. Lett. **80**, 4190 (2002).
[12] W. Rave, K. Fabian, and A. Hubert, J. Magn. Magn. Mater. **190**, 332 (1998).
[13] K. L. Metlov and K. Yu. Guslienko, J. Magn. Magn. Mater. **242**, 1015 (2002).
[14] A. Hubert and R. Schäfer, *Magnetic Domains* (Springer, Berlin, Heidelberg, 1998).
[15] L. D. Buda, I. L. Prejbeanu, U. Ebels, and K. Ounadjela, Comput. Mater. Sci. **24**, 181 (2002).
[16] Y. Murayama, J. Phys. Soc. Jpn. **21**, 2253 (1966).
[17] M. Hehn, R. Ferré, K. Ounadjela, J.-P. Bucher, and F. Rousseaux, J. Magn. Magn. Mater. **165**, 5 (1997).
[18] N. Saito, H. Fujiwara, and Y. Sugita, J. Phys. Soc. Jpn. **19**, 1116 (1964).
[19] J. Ben Youssef, N. Vukadinovic, D. Billet, and M. Labrune, Phys. Rev. B **69**, 174402 (2004).
[20] N. Vukadinovic, O. Vacus, M. Labrune, O. Acher, and D. Pain, Phys. Rev. Lett. **85**, 2817 (2000).
[21] K. Yu. Guslienko, B. A. Ivanov, V. Novosad, Y. Otani, H. Shima, and K. Fukamichi, J. Appl. Phys. **91**, 8037 (2002).
[22] J. P. Park, P. Eames, D. M. Engebretson, J. Berezovsky, and P. A. Crowell, Phys. Rev. B **67**, 020403(R) (2003).
[23] J. P. Park and P. A. Crowell, Phys. Rev. Lett. **95**, 167201 (2005).
[24] X. Zhu, Z. Liu, V. Metlushko, P. Grütter, and M. R. Freeman, Phys. Rev. B **71**, 180408(R) (2005).
[25] M. Buess, T. P. J. Knowles, R. Höllinger, T. Haug, U. Krey, D. Weiss, D. Pescia, M. R. Scheinfein, and C. H. Back, Phys. Rev. B **71**, 104415 (2005).
[26] D. D. Sheka, J. P. Zagorodny, J.-G. Caputo, Yu. Gaididei, and F. G. Mertens, Phys. Rev. B **71**, 134420 (2005).
[27] F. J. Castaño, C. A. Ross, C. Frandsen, A. Eilez, D. Gil, H. I. Smith, M. Redjdal, and F. B. Humphrey, Phys. Rev. B **67**, 184425 (2003).
[28] S. Komineas, J. Phys. A **39**, 5669 (2006).
[29] S. Komineas and N. Papanicolaou, Nonlinearity **11**, 265 (1998).